arXiv:1404.3607v1 [cond-mat.mes-hall] 14 Apr 2014

Spontaneous Layer-Pseudospin Domain Walls in Bilayer Graphene

Xiao Li,[1] Fan Zhang,[2,*] Qian Niu,[1,3] and A. H. MacDonald[1]

[1] *Department of Physics, The University of Texas at Austin, Austin, Texas 78712, USA*
[2] *Department of Physics and Astronomy, University of Pennsylvania, Philadelphia, PA 19104, USA*
[3] *International Center for Quantum Materials, and Collaborative Innovation Center of Quantum Matter, School of Physics, Peking University, Beijing 100871, China*

Bilayer graphene is susceptible to a family of unusual broken symmetry states with spin and valley dependent layer polarization. We report on a microscopic study of the domain walls in these systems, demonstrating that they have interesting microscopic structures related to order-induced topological characters. We use our results to estimate Ginzburg-Landau model parameters and transition temperatures for the ordered states of bilayer graphene.

Introduction.— Neutral bilayer graphene (BLG) [1, 2] and its ABC-stacked multilayer cousins [3–6], are attractive platforms for unconventional two-dimensional electron systems physics because they have flat band contact near their Fermi levels, and because order induces large momentum-space Berry curvatures [6] in their quasiparticle bands. Theoretical studies have identified a variety of potential broken symmetry states in neutral suspended BLG [6–29]. The band eigenstates in bilayer graphene are equal weight coherent sums of components localized in each layer, and have an interlayer phase that is strongly wavevector dependent. When lattice-scale corrections to bilayer graphene's massive Dirac model [1, 2] are neglected, the broken symmetry states predicted by mean-field theory have a charged quasiparticle energy gap [6, 7, 10–12] and spontaneous layer polarization within each of the four spin-valley flavors. Recent experiments [30–38] appear to rule out a competing family of nematic states [13–15], which do not have a quasiparticle gap and break rotational symmetry [39].

The theoretical expectation [6–9] is that long-range Coulomb interactions should favor the subset of broken symmetry states with no overall layer-polarization. Recent experiments [38] utilize Zeeman response to an in-plane magnetic field [16] to identify the ground state as either a layer antiferromagnet [6] in which opposite spins have opposite layer polarization, or a quantum spin Hall insulator [6, 9] in which layer polarization changes when either spin or valley is reversed. (In mean field theories the former state is favored by lattice scale exchange interactions [8].) In this Letter we present a microscopic theory of domain walls in which the sense of layer polarization of one flavor is reversed, focusing on the unusual properties associated with the ordered states' topological characters. These domain walls proliferate thermally above an Ising phase transition temperature which we estimate and, because they can be induced by spatial variations in the potential difference between layers, are expected to be common in bilayer graphene samples.

Continuum model mean-field theory.— We first establish our notation by discussing uniform chiral symmetry breaking in BLG in terms of the ordered state quasiparticle Hamiltonians [6] suggested by mean-field calculations and renormalization group analyses [7, 8, 10–12, 16–18]:

$$\begin{aligned}\mathcal{H}^{HF} &= \sum_{\boldsymbol{k}\alpha\beta ss'} c^\dagger_{\boldsymbol{k}\alpha s}\big[h_0 + h_F\big]c_{\boldsymbol{k}\beta s'}\,,\\ h_0 &= -\epsilon_{\boldsymbol{k}}\big[\cos(2\phi_{\boldsymbol{k}})\sigma_x^{\alpha\beta} + \sin(2\phi_{\boldsymbol{k}})\sigma_y^{\alpha\beta}\big]\delta_{ss'}\,,\\ h_F &= -\big[V_0 + V_z\sigma_z^{\alpha\alpha}\sigma_z^{\beta\beta}\big]\,\Delta^{\beta s'}_{\alpha s}\,.\end{aligned} \tag{1}$$

Here Greek letters label layer, s and s' label spin, $\epsilon_{\boldsymbol{k}} = (v_{\rm SL}\hbar k)^2/\gamma_1$ is the band dispersion, $v_{\rm SL}$ is the single-layer Dirac-model velocity, γ_1 is the interlayer hopping energy, $\cot\phi_{\boldsymbol{k}} = \tau_z k_x/k_y$ with $\tau_z = \pm 1$ denoting valleys K and K', and $V_{0,z} = (V_s \pm V_d)/2$ is the sum and difference of the same (s) and different (d) layer interactions, which for convenience we assume to be short-ranged. The order parameters $\Delta^{\beta s'}_{\alpha s} = A^{-1}\sum_{\boldsymbol{k}}\langle c^\dagger_{\boldsymbol{k}\beta s'}c_{\boldsymbol{k}\alpha s}\rangle_f$ must be determined self-consistently. Note that in using short-range interactions we are assuming that the screened Coulomb interaction range is short relative to the short-distance cut-off of the two-band continuum model, $v_{\rm SL}\hbar/\gamma_1$, but much larger than the graphene lattice constant. The form used for the mean-field Hamiltonian in Eq. (1) has been simplified by noting that the mean-field ground state has no net layer polarization, and that the mean-field interaction vertices are diagonal in layer [16]. This Hamiltonian generates a family of states differing only in the flavor dependence of the sign of interaction-generated mass terms proportional to $m_z\sigma_z^{\alpha,\beta}$. In this Letter we concentrate on domain walls formed within a single flavor, reserving comments on the role of spin and valley degrees-of-freedom to the end of the article.

The gap equation can be solved to yield an implicit solution for m_z:

$$1 = \nu_0 V_s \int_0^{\gamma_1} \frac{1}{2\varepsilon}[f(-\varepsilon-\mu) - f(\varepsilon-\mu)]d\varepsilon\,, \tag{2}$$

where $\nu_0 = \gamma_1/(4\pi\hbar^2 v_{\rm SL}^2)$ is the band density-of-states per flavor, γ_1 is the continuum model ultraviolet cut-off energy, μ is the Fermi energy, $\varepsilon = \sqrt{\epsilon_{\boldsymbol{k}}^2 + m_z^2}$, and $f(\varepsilon) = (1 + e^{\varepsilon/k_BT})^{-1}$ is the Fermi function. For charge-neutral BLG and $m_z \ll \gamma_1$, we find that the quasiparticle gap is $2m_z = 4\gamma_1\exp(-2/V_s\nu_0)$ at zero temperature, and

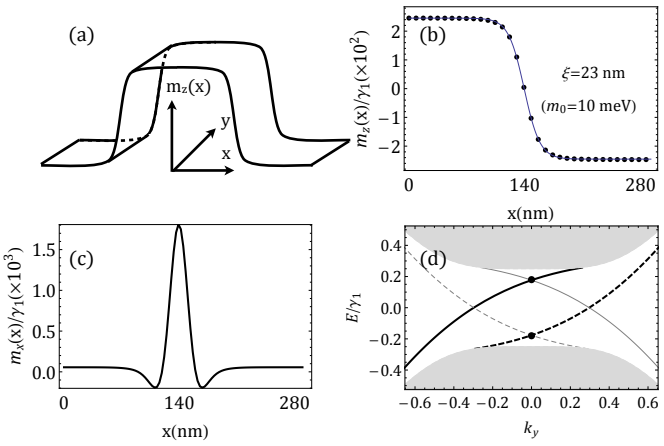

FIG. 1. (a) Schematic summary of our domain wall calculations. These domain walls (kink and antikink) are oriented along the y direction and the mass changes sign along the x direction. (b)-(c) Typical mean-field solutions for $m_z(x)$ and $m_x(x)$ variation across a domain wall. Note the different scales in (b) and (c). (d) Energy spectrum of a model with sharp domain walls. The gray area is the bulk continuum. Black and gray lines are used to distinguish chiral states localized at the domain walls which propagate in opposite directions while solid and dashed lines are used to distinguish states with $\langle\sigma_x\rangle < (>) 0$. The two black dots identify the states with $E = \pm|m_0|/\sqrt{2}$ discussed in the text.

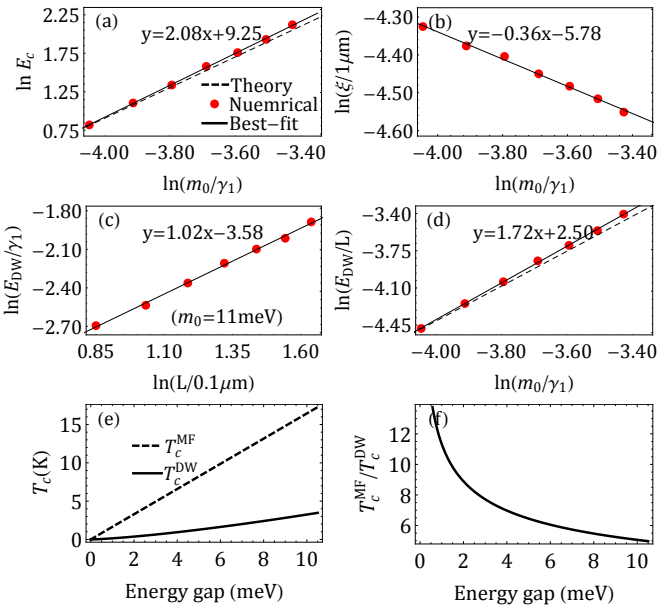

FIG. 2. Microscopic domain wall properties for square simulation cells with side L. Calculations were performed as a function of L and the interaction strength, and the results are plotted as a function of L and the mass m_0 that interaction strength yields in the ground state. The uniform system energy gap is $2m_0$. In these figures, red dots are numerical data, while the thin solid lines are power law fits. (a) Condensation energy $E_{\rm cond}$ of bilayer graphene (in units $\gamma_1/\mu{\rm m}^2$) as a function of m_0. The dashed line is obtained from analytical results. (b) Domain wall width ξ as a function of m_0. (c) Domain wall energy $E_{\rm DW}$ as a function of L. (d) Domain wall surface tension $J \equiv E_{\rm DW}/L$ (in units of $\gamma_1/0.1\mu{\rm m}^2$) as a function of m_0. The dashed line is the GL theory prediction for the domain wall surface tension. (e) and (f) Comparison of the collective $T_c^{\rm DW}$ and mean-field $T_c^{\rm MF}$ critical temperature estimates discussed in the text.

that m_z vanishes at $T = T_c^{\rm MF}$ where

$$T_c^{\rm MF} = e^{\gamma} m_z/\pi k_B\,, \tag{3}$$

and γ is Euler's constant.

Microscopic theory of domain walls.— We now consider the microscopic electronic structure of the domain walls that separate regions with opposite layer-polarization signs. These domain walls are quite different from those of an easy axis ferromagnet, for example, because the layer-pseudospin dependent term in the band Hamiltonian is not a small correction to an otherwise pseudospin independent Hamiltonian. In order to use periodic boundary conditions we must, as illustrated in Fig. 1(a), allow for two adequately separated domain walls along the direction in which we allow the sign of mass to change. We use a plane-wave expansion method to solve the spatially inhomogeneous gap equations. The interaction terms in the mean-field Hamiltonian are spatially local and can be parameterized in terms of position dependent masses $m_i(x)$ associated with the three Pauli matrices σ_i. For short-range interactions, their plane-wave matrix elements are

$$m_i(k_1', k_1) = \frac{V_s}{2A} \sum_{f\alpha\beta,\boldsymbol{q}} \langle c^\dagger_{k_1'\hat{x}+\boldsymbol{q},\alpha} \sigma_i^{\alpha\beta} c_{k_1\hat{x}+\boldsymbol{q},\beta}\rangle_f\,, \tag{4}$$

where $i = x, y, z$, and f labels filled quasiparticle states. Note that the mass terms depend on $k_1' - k_1$ only. The inverse Fourier transform of this function specifies $m_i(x)$.

These self-consistent gap equations are readily solved. Results for finite square simulation cells of side L are summarized in Fig. 1 and Fig. 2. A typical result for the domain wall m_z profile, plotted in Fig. 1(b), can be accurately fit to the form $m_z(x) = m_0 \tanh[(x - x_0)/\sqrt{2}\xi]$, where $2m_0$ is the quasiparticle gap and x_0 is the position of the domain wall center. As illustrated in Fig. 2(a) and (b), the energy cost of a domain wall $E_{\rm DW}$ in our numerical calculation is accurately proportional to L, indicating that finite-size effects are not playing a large role. Fig 2(c) illustrates our finding that the domain wall energy per unit length (the two-dimensional *surface tension*) $J = E_{\rm DW}/L$ and the domain wall width ξ have power law dependences on the uniform system mass m_0: $J \sim m_0^\alpha$ and $\xi \sim m_0^\beta$ with with $\alpha = 1.72$ and $\beta = -0.36$. The surface tension increases and the domain wall width decreases with increasing m_0.

Interlayer coherence response— The band states of bilayer graphene are coherent combinations [2] of top and bottom layer components with an interlayer phase ϕ that is twice the momentum orientation angle $\phi_{\boldsymbol{k}}$. When rep-

resented by layer-pseudospins, valence band states are in the x-y plane and have orientation angle $\phi = 2\phi_{\boldsymbol{k}}$. The m_x and m_y pseudospin magnetizations of both gapped and ungapped states therefore vanish after summing over momenta. As illustrated in Fig 1(c), our numerical calculations have revealed that a finite net in-plane pseudospin magnetization develops inside domain walls with a magnitude typically one order smaller than m_0. The in-plane pseudospin magnetization is oriented across the domain wall, *i.e.*, in the x-direction for the geometry we have chosen. Intriguingly, the sign of m_x is the same for both kink and anti-kink domain walls. This in-plane pseudospin magnetization cannot be understood in terms of gradient expansions based on uniform system quasiparticle linear response functions since $\chi_{xz}(\boldsymbol{q}) = \chi_{yz}(\boldsymbol{q}) = 0$.

Near a domain wall, the sign of m_z is reversed and the local Chern number changes by two [6, 42, 43], giving rise to two chiral zero modes per valley propagating along the domain wall, as illustrated in Fig. 1(d). We attribute the finite m_x value in the domain wall to the properties of the topological edge states it traps, as we now explain. At any value of k_y the mean-field Hamiltonian $\mathcal{H}$ in the presence of domain walls is invariant under simultaneous rotation by 180° around the pseudo spin $\hat{x}$ axis and mirror transformation $x \to -x$ through the domain wall: $\sigma_x \mathcal{H} \sigma_x = \mathcal{H}(-\partial_x, -x)$. Here we assume that $x = 0$ is chosen to lie at the mid-point of a single domain wall. It follows that for any k_y, the two components of the eigenstates $\psi(x) = [u(x), v(x)]^{\mathrm{T}}$ satisfy $v(x) = \pm u(-x)$, and hence that the pseudospin operator σ_x will have a non-zero expectation value near $x = 0$. Similarly since $\sigma_y \mathcal{H}(k_y) \sigma_y = -\mathcal{H}(-k_y)$, if $(u, v)^{\mathrm{T}}$ is an eigenstate of $\mathcal{H}$ at k_y with eigenvalue E, then $(v, -u)^{\mathrm{T}}$ is an eigenstate at $-k_y$ with eigenvalue $-E$. It follows that the two chiral states with $E = 0$ will appear at opposite values of k_y and have opposite expectation values of $\langle \sigma_x \rangle$. For example in the case of a sharp kink, *i.e.*, for $m_z(x) = m_0 \,\mathrm{sgn}(x)$, the chiral states at $k_y = 0$ have $E = \pm |m_0|/\sqrt{2}$ (lying in the gap) and $\langle \sigma_x \rangle = \mp 1$. Although the edge states are not fully polarized in the general case, states within a given chiral state branch have non-zero values of $\langle \sigma_x \rangle$ with a common sign and the edge state occupations are generically different for any position of the chemical potential within the uniform state mass gap.

Typical behavior is illustrated in Fig. 1(d). The dashed and solid edge state branches have different signs of $\langle \sigma_x \rangle$ and different occupations. As a consequence, $m_x(x)$ exhibits a positive peak at each domain wall center. This in-plane pseudospin magnetization is independent of the domain wall sign and valley index, and thus survives summation over flavors for any gapped broken symmetry state that breaks chiral symmetry within flavors [6]. We note that this nonlinear response also arises near electric field driven domain walls [42–50] and layer stacking domain walls [43–45].

Phenomenological theory of domain walls.— The domain wall shape found in our numerical calculations is consistent [40, 41] with the Ising-order Ginzburg-Landau-theory energy functional

$$F = \int d^2\vec{r} \left[\frac{c}{2} (\nabla m_z)^2 + \mathcal{V}[m_z(x)] - E_c \right], \qquad (5)$$

where $\mathcal{V}[m_z] = -r m_z(x)^2/2 + u m_z(x)^4$ with both r and u positive, and $E_c = -r^2/16u$ is the condensation energy per unit area of the uniform m_z ground state. We include the constant E_c in this expression so that the minimum value of F, which occurs for constant masses $m_z^* = \pm m_0 = \pm (r/4u)^{1/2}$, is zero. For a single domain wall configuration in which $m_z \to \pm m_0$ for $x \to \pm\infty$, the functional (5) is minimized by $m_z(x) = \pm m_0 \tanh[(x - x_0)/\sqrt{2}\xi]$ with $\xi = \sqrt{c/r}$. The three independent parameters of the Ginzburg-Landau model reproduce microscopic values for m_0, ξ, and E_c when we set $c = 4E_c\xi^2/m_0^2$, $r = 4E_c/m_0^2$, and $u = E_c/m_0^4$. In Fig. 2(a) we demonstrate that the GL theory expression for the domain wall surface tension $J = 8\sqrt{2}\xi E_c/3$ agrees accurately with our microscopic calculations, and that the power laws relating ξ and J to the microscopic gap satisfy $\alpha - \beta = 2$, also in agreement with the GL theory.

Ising critical temperature estimate— We now utilize the above results to estimate the critical temperature T_c^{DW} above which domain walls nucleated by thermal fluctuations proliferate and Ising long-range order within flavors is lost. For this purpose we follow a common physical argument [40] which compares the energy cost associated with domain wall nucleation with the corresponding entropic free energy gain. The energy cost to form a domain wall with perimeter P in the uniform state is JP, whereas the entropy is $k_B \ln C_P$, where C_P is the number of distinct closed-loop non-intersecting P/W-step walks. Here $W = 2\sqrt{2}\xi$ [40] is the minimum distance over which a domain wall can change direction. Using $C_P = (1 + \sqrt{2})^{P/W}$ [40], we find that for temperatures above $T_c^{\mathrm{DW}} = WJ/(k_B \ln(1 + \sqrt{2}))$, the proliferation of domains separating regions with different layer polarization signs is thermodynamically favored and long-range order is lost. Combining our numerical results for ξ and J yields

$$\frac{k_B T_c^{\mathrm{DW}}}{m_0} = \frac{0.64}{\ln(1 + \sqrt{2})} (m_0/\gamma_1)^{\alpha+\beta-1}. \qquad (6)$$

Since $\alpha + \beta - 1 > 0$ and $m_0 \ll \gamma_1$, $k_B T_c^{\mathrm{DW}} \ll m_0$.

We have so far ignored thermal fermionic fluctuations which produce particle-hole excitations and would limit the critical temperature if the domain wall energy was very large. Because the mean-field theory gap equation is identical to that of BCS theory, it implies a critical temperature limit that is proportional to m_0. As illustrated in Fig. 2 (e) and (f), the ratio $T_c^{\mathrm{MF}}/T_c^{\mathrm{DW}}$ decreases with increasing m_0 in agreement with Eq. (6). Noting that $\gamma_1 \sim 400\,\mathrm{meV}$ and that experimental [35] values of

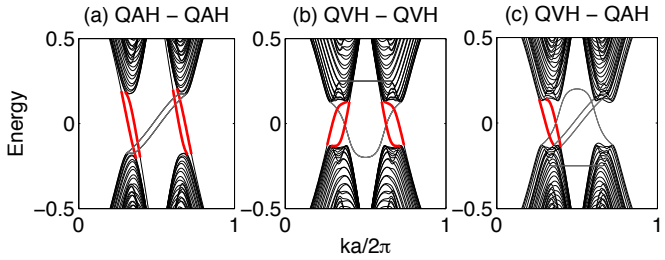

FIG. 3. Distinct domain wall zero-line patterns in gapped bilayer graphene samples which do not break spin-rotational symmetry. The red lines denotes the zero modes localized at domain walls between (a) two QAH regions with opposite total Hall conductance, (b) two QVH regions with opposite layer polarization, and (c) a QVH and a QAH region. The gray lines represent the edge states on the outermost zigzag boundaries. Note that they are doubly degenerate in (a) and (b). These figures were constructed using a tight-binding model of the gapped states.

m_0 in bilayer graphene are always smaller than 4 meV, we conclude that the temperature to which spontaneous layer polarization order survives is limited in practice by domain wall nucleation.

Discussion.— It is instructive to compare spontaneously gapped bilayer graphene with BCS superconductors. In both cases weak interaction instabilities lead to a linear dependence of $T_c^{\rm MF}$ on the gap parameter m_0. Collective properties differ qualitatively however, in the first place because of the difference between the order parameter dimensions. In superconductors the collective excitations whose proliferation limits the critical temperature are vortices rather than domain walls. Additionally the free fermion dispersion is linear near the Fermi energy in the superconductor case but *quadratic* in bilayer graphene. As a result, the coherence length in superconductors is related to the gap Δ by $\xi \sim \hbar v_{\rm SL}/\Delta$, and the collective limit on the temperature must therefore exceed the nucleation energy of a vortex, *i.e.*, $k_B T_c \sim E_c \xi^2 \sim \varepsilon_F$, independent of and much larger than the gap or the mean-field critical temperature estimate. A similar estimate of the collective limit on T_c can be obtained by appealing to Kosterlitz-Thouless theory, which explains why critical temperatures of weakly disordered superconducting thin films are accurately predicted by mean-field theory. In bilayer graphene on the other hand, the relationship between ξ and the gap can be estimated using $m_0 \sim (\hbar v_{\rm SL}/\xi)^2/\gamma_1$. This estimate yields $\beta = -0.5$, in rough agreement with the estimate $\beta = -0.36$ extracted from our numerical results. It follows that for bilayer graphene, the collective fluctuation critical temperature estimate is comparable to mean-field-theory estimate, and becomes smaller in systems with small gaps. Unlike the case of superconductors, collective order parameter fluctuations play an important role in limiting the critical temperature in bilayer graphene.

When the four spin-valley flavors and weak valley dependence of electron-electron interactions are taken into account, the $2^4 = 16$ gapped broken symmetry states that are close in energy [8] can be classified into 5 distinct phases [6]. This in turn leads to 16 distinct types of domain walls. In Fig. 3 we illustrate only the cases in which spin rotational invariance is not broken. In this case only the quantum valley Hall (QVH) state and quantum anomalous Hall (QAH) state are allowed, and support two intra-phase and one inter-phase domain wall. Because the valley-projected Chern numbers are almost quantized [6, 42, 43, 50] to ± 1 in these states, all domain walls support chiral edge states. At a domain wall separating two QAH regions with opposite total Hall conductances, as illustrated in Fig. 3(a), the Chern number changes have the same sign for both valleys, yielding four modes with the same chirality. At a domain wall separating two QVH regions with opposite layer polarization, the Chern numbers change by ± 2, with opposite signs for opposite valleys. Thus two chiral zero modes (per spin) appear at valley K and two with opposite chirality at the valley K', as illustrated in Fig. 3(b). This type of domain wall can be easily realized using an external electric field [42–50] or a stacking fault [43–46]. Finally, at the domain wall between a QVH and a QAH regions the Chern number is changed by two for one valley while it is unchanged for the other. Thus the zero modes at the domain wall are chiral in one valley and absent in the other. In all these cases, edge modes have a double spin-degeneracy. States in which spin-rotational invariance is also broken can be similarly analyzed. Each of the 16 types of domain wall hosts a Luttinger liquid [51] with distinct properties. We emphasize that inter-valley scattering, ignored in the discussion above, should be extremely weak in the high quality samples required for the appearance of spontaneously gapped states, as the domain wall widths we obtain are much larger than the graphene lattice constant. Our work suggests that large-area bilayer graphene gapped states should exhibit interesting transport anomalies and their critical behaviors [52]. Similar phenomena will occur in thicker ABC-stacked few-layer [6] graphene systems which have larger spontaneous gaps [32, 33] and more robust domain walls.

Acknowledgements.— X.L. acknowledges Z. Qiao, H. Chen and M. Xie for helpful technical advice and is supported by NBRPC (No. 2012CB921300 and No. 2013CB921900) and NSFC (No. 91121004) during his visit at Peking University. F.Z. is indebted to C. Kane and E. Mele for helpful discussions and is supported by DARPA Grant No. SPAWAR N66001-11-1-4110. Q.N. is supported in part by DOE-DMSE (No. DE-FG03-02ER45958) and the Welch Foundation (No. F-1255). A.H.M. is supported by the Welch Foundation under Grant No. TBF1473 and by the DOE Division of Materials Sciences and Engineering under grant No. DE-FG03-02ER45958.

* E-mail: zhf@sas.upenn.edu

[1] A. H. Castro Neto, F. Guinea, N. M. R. Peres, K. S. Novoselov, and A. K. Geim, Rev. Mod. Phys. **81**, 109 (2009).

[2] E. McCann and V. I. Fal'ko, Phys. Rev. Lett. **96**, 086805 (2006).

[3] H. Min and A. H. MacDonald, Phys. Rev. B **77**, 155416 (2008).

[4] M. Koshino and E. McCann, Phys. Rev. B **80**, 165409 (2009).

[5] F. Zhang, B. Sahu, H. Min, and A. H. MacDonald, Phys. Rev. B **82**, 035409 (2010).

[6] F. Zhang, J. Jung, G. A. Fiete, Q. Niu, and A. H. MacDonald, Phys. Rev. Lett. **106**, 156801 (2011).

[7] H. Min, G. Borghi, M. Polini, and A. H. MacDonald, Phys. Rev. B **77**, 041407(R) (2008).

[8] J. Jung, F. Zhang, and A. MacDonald, Phys. Rev. B **83**, 115408 (2011).

[9] R. Nandkishore and L. Levitov, Phys. Rev. B **82**, 115124 (2010).

[10] F. Zhang, H. Min, M. Polini, and A. H. MacDonald, Phys. Rev. B **81**, 041402(R) (2010).

[11] R. Nandkishore and L. Levitov, Phys. Rev. Lett. **104**, 156803 (2010).

[12] F. Zhang, H. Min, and A. H. MacDonald, Phys. Rev. B **86**, 155128 (2012).

[13] O. Vafek and K. Yang, Phys. Rev. B **81**, 041401(R) (2010).

[14] Y. Lemonik, I.L. Aleiner, C. Toke, and V.I. Fal'ko, Phys. Rev. B **82**, 201408(R) (2010).

[15] A. S. Mayorov, D. C. Elias, M. Mucha-Kruczynski, R. V. Gorbachev, T. Tudorovskiy, A. Zhukov, S. V. Morozov, M. I. Katsnelson, V. I. Fal'ko, A. K. Geim, and K. S. Novoselov, Science **333**, 860 (2011).

[16] F. Zhang and A. H. MacDonald, Phys. Rev. Lett. **108**, 186804 (2012).

[17] A. H. MacDonald, J. Jung, and F. Zhang, Phys. Scr. **T146**, 014012 (2012).

[18] M. M. Scherer, S. Uebelacker, and C. Honerkamp, Phys. Rev. B **85**, 235408 (2012).

[19] T. C. Lang, Z. Meng, M. M. Scherer, S. Uebelacker, F. F. Assaad, A. Muramatsu, C. Honerkamp, and S. Wessel, Phys. Rev. Lett. **109**, 126402 (2012).

[20] R. Nandkishore and L. Levitov, Phys. Rev. B **82**, 115431 (2010).

[21] O. Vafek, Phys. Rev. B **82**, 205106 (2010).

[22] M. Trushin and J. Schliemann, Phys. Rev. Lett. **107**, 156801 (2011).

[23] M. Trushin and J. Schliemann, New J. Phys. **14**, 095005 (2012).

[24] M. Y. Kharitonov, Phys. Rev. B **86**, 195435 (2012).

[25] E. V. Gorbar, V. P. Gusynin, V. A. Miransky, and I. A. Shovkovy, Phys. Rev. B **86**, 125439 (2012).

[26] R. E. Throckmorton and O. Vafek, Phys. Rev. B **86**, 115447 (2012).

[27] V. Cvetkovic, R. E. Throckmorton, and O. Vafek, Phys. Rev. B **86**, 075467 (2012)

[28] Y. Lemonik, I. L. Aleiner, and V. I. Fal'ko, Phys. Rev. B **85**, 245451 (2012).

[29] L. Zhu, V. Aji, and C. M. Varma, Phys. Rev. B **87**, 035427 (2013).

[30] J. Martin, B. E. Feldman, R. T. Weitz, M. T. Allen, and A. Yacoby, Phys. Rev. Lett. **105**, 256806 (2010).

[31] R. T. Weitz, M. T. Allen, B. E. Feldman, J. Martin, and A. Yacoby, Science **330**, 812 (2010).

[32] W. Bao, L. Jing, J. Velasco Jr, Y. Lee, G. Liu, D. Tran, B. Standley, M. Aykol, S. B. Cronin, D. Smirnov, M. Koshino, E. McCann, M. Bockrath, and C. N. Lau, Nature Physics **7**, 948 (2011).

[33] Y. Lee, D. Tran, K. Myhro, J. Velasco Jr., N. Gillgren, C. N. Lau, Y. Barlas, J. M. Poumirol, D. Smirnov, F. Guinea, eprint arXiv:1402.6413 (2014).

[34] F. Freitag, J. Trbovic, M. Weiss, and C. Schönenberger, Phys. Rev. Lett. **108**, 076602 (2012).

[35] J. J. Velasco, L. Jing, W. Bao, Y. Lee, P. Kratz, V. Aji, M. Bockrath, C. Lau, C. Varma, R. Stillwell, D. Smirnov, F. Zhang, J. Jung, and A. MacDonald, Nature Nanotechnology, **7**, 156 (2012).

[36] W. Bao, J. Velasco Jr, F. Zhang, L. Jing, B. Standley, D. Smirnov, M. Bockrath, A. H. MacDonald, and C. N. Lau, Proc. Natl. Acad. Sci. USA, **109**, 10802 (2012).

[37] A. Veligura, H. J. van Elferen, N. Tombros, J. C. Maan, U. Zeitler, and B. J. van Wees, Phys. Rev. B **85**, 155412 (2012).

[38] F. Freitag, M. Weiss, R. Maurand, J. Trbovic, and C. Schönenberger, Phys. Rev. B **87**, 161402(R) (2013).

[39] G. Dávid, P. Rakyta, L. Oroszlány, and & J. Cserti, Phys. Rev. B 85, 041402(R) (2012).

[40] P. M. Chaikin and T. C. Lubensky, Principles of Condensed Matter Physics, reprint ed. (Cambridge University Press, 2000).

[41] M. Tinkham, Introduction to Superconductivity, 2nd ed. (Courier Dover Publications, 2012).

[42] I. Martin, Y. M. Blanter, and A. F. Morpurgo, Phys. Rev. Lett. **100**, 036804 (2008).

[43] F. Zhang, A. H. MacDonald, and E. J. Mele, Proc. Natl. Acad. Sci. USA **110**, 10546 (2013).

[44] J. S. Alden, A. W. Tsen, P. Y. Huang, R. Hovden, L. Brown, J. Park, D. A. Muller, and P. L. McEuen, Proc. Natl. Acad. Sci. USA **110**, 11256 (2013).

[45] A. Vaezi, Y. Liang, D. H. Ngai, L. Yang, and E. Kim, Phys. Rev. X **3**, 021018 (2013).

[46] W. Yao, S. A. Yang, and Q. Niu, Phys. Rev. Lett. **102**, 096801 (2009).

[47] J. Jung, F. Zhang, Z. Qiao, and A. H. MacDonald, Phys. Rev. B **84**, 075418 (2011).

[48] Z. Qiao, J. Jung, Q. Niu and A. H. MacDonald, Nano Lett. **11**, 3453 (2011).

[49] M. Zarenia, J. M. Pereira, Jr., G. A. Farias, and F. M. Peeters, Phys. Rev. B, **84**, 125451 (2011).

[50] J. Li, I. Martin, M. Buttiker, and A. F. Morpurgo, Nature Phys. **7**, 38 (2011).

[51] M. Killi, T. Wei, I. Affleck, and A. Paramekanti, Phys. Rev. Lett. **104**, 216406 (2010).

[52] B. J. Wieder, F. Zhang, and C. L. Kane, to publish soon.